

OPAL 2: Rapid Optical Simulation of Silicon Solar Cells

Keith R. McIntosh and Simeon C. Baker-Finch

PV Lighthouse, Coledale, NSW 2515, Australia

The following pages contain the accepted version of the paper that introduces OPAL 2. It is published in the proceedings of the 38th IEEE Photovoltaic Specialists Conference, Austin, 2012.

The top plot in Figure 6 of the accepted and published versions of the paper is incorrect. Here is a corrected version of Figure 6.

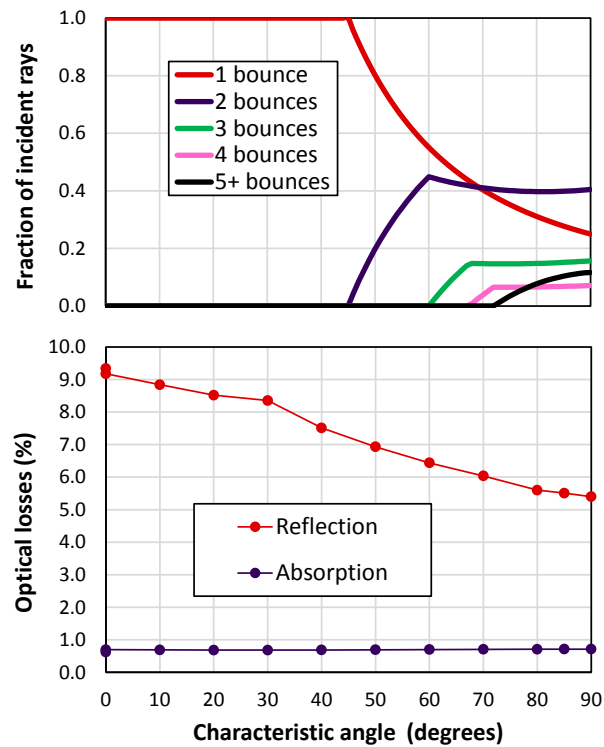


Fig. 6. (a) Fraction of incident rays that bounce once, twice, etc. at the front surface, and (b) reflection and ARC absorption vs ω for spherical caps. Simulation details described in the text.

OPAL 2: Rapid Optical Simulation of Silicon Solar Cells

Keith R. McIntosh and Simeon C. Baker-Finch

PV Lighthouse, Coledale, NSW 2515, Australia

Abstract — The freeware program OPAL 2 computes the optical losses associated with the front surface of a Si solar cell. It calculates the losses for any angle of incidence within seconds, where the short computation time is achieved by decoupling the ray tracing from the Fresnel equations. Amongst other morphologies, OPAL 2 can be used to assess the random-pyramid texture of c-Si solar cells, or the ‘isotexture’ of mc-Si solar cells, and to determine (i) the optimal thickness of an antireflection coating with or without encapsulation, (ii) the impact of imperfect texturing, such as non-ideal texture angles, over-etched isotexture, and flat regions, and (iii) the subsequent 1D generation profile in the Si. This paper describes the approach and assumptions employed by OPAL 2 and presents examples that demonstrate the dependence of optical losses on texture quality and incident angle.

Index Terms — Antireflection coatings, Optical losses, Ray Tracing, Silicon, Software, Surface texture.

I. INTRODUCTION

Antireflection coatings (ARCs) and surface texture greatly enhance a solar cell’s capacity to absorb sunlight. Both features also complicate the assessment of its optics.

In the first case, an ARC introduces interference. Reflection, absorption and transmission are therefore dependent on the thickness, refractive index $n(\lambda)$ and extinction coefficient $k(\lambda)$ of the ARC. Moreover, the interference depends on $n(\lambda)$ of the overlying layer (e.g., EVA) and $n(\lambda)$ and $k(\lambda)$ of the underlying semiconductor (e.g., Si). Complicating matters further, the interference depends on the angle and polarization of the incident light, an ARC can consist of multiple films, and $n(\lambda)$ and $k(\lambda)$ can vary significantly with wavelength λ .

In the second case, surface texture causes light to reflect multiple times from the front surface. Thus, reflection, absorption and transmission must be calculated for each ‘bounce’ of light, and combined correctly to determine the total reflection, absorption and transmission. In so doing, it is necessary to calculate how the texture alters the angle of incidence and the polarization of the light.

The complexity of the optical structure can be solved via geometrical ray tracing when features are large enough to render diffractive effects negligible. Many ray tracing programs, however, do not account for non-zero extinction coefficients or polarization.

In 2010, we introduced OPAL, a freeware program that accurately models multiple interactions of normally incident light with surface texture, that accounts for λ -dependent complex refractive indices, and that implements a rigorous approach to the analysis of the polarization of rays as they interact with the structure [1, 2]. The program also calculates

the resulting generation current J_G within the underlying substrate for a user-defined spectrum, thereby permitting ARC optimization via maximizing J_G .

In this paper we present OPAL 2, which extends the functionality to include

- illumination of any angle of incidence and polarization;
- hillocks (octagon-based pyramids), which can arise under some processing conditions on c-Si [3–5];
- spherical caps, which have been demonstrated to approximate isotextured mc-Si [6, 7];
- V grooves;
- imperfect texture, whereby pyramids, hillocks and spherical caps have a non-ideal characteristic angle, as occurs in practical solar cells [3, 7]; and
- incomplete texture, where a user-defined proportion of the wafer is textured and the remainder is planar.

OPAL 2 also contains a larger database of $n(\lambda)$ and $k(\lambda)$ for optical materials, calculates an approximate 1D generation profile, calculates J_{SC} for a given $IQE(\lambda)$, and is faster.

In this paper, we first reiterate the general approach taken by the freeware program including the assumptions that underlie the aforementioned extensions. We demonstrate its application to practical Si solar cells by determining the optical losses for random pyramids, random hillocks and spherical caps over a range of characteristic angles, incident angles, and planar fractions. The program is free and available online [8].

II. APPROACH AND ASSUMPTIONS

There are three principal components to OPAL 2: ray tracing, thin-film optics; and equivalent-current calculations.

A. Ray tracing

In generic ray tracing programs, reflection, absorption and transmission (RAT) are usually calculated at every interaction of every ray. When thin-film coatings are included, this leads to relatively long computation times because the Fresnel equations are solved at every interaction.

By contrast, OPAL recognizes that the number of ‘unique paths’ is small, where all rays within a unique path reflect from the same facets at the same angles and must therefore have the same RAT. Thus, the Fresnel equations need only be solved for each path, not for every ray. In fact, some paths are subsets of other paths, making the number of necessary computations even smaller; and some paths that impinge on

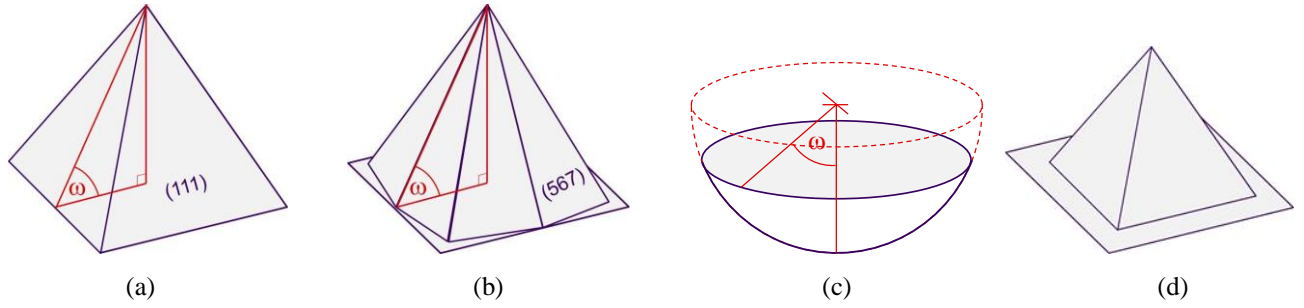


Fig. 2. (a) An upright pyramid, (b) a hillock, and (c) a spherical cap, where ω denotes the characteristic angle; and (d) an example of a ‘distributed’ planar region about an upright pyramid, where the sides of the pyramid are equidistant from the planar square.

different facets are effectively identical under a certain polarization, making the number of unique paths smaller still.

A simple example is regular upright pyramids with $\omega = 54.74^\circ$ under normally incident unpolarized light. In this case, 88.8% of rays reflect twice from opposing pyramid facets at angles of 54.74° and 15.79° , while 11.1% reflect three times at 54.74° , 15.79° and 86.32° [9]. Moreover, unpolarized light striking any of the four pyramid facets gives the same RAT due to the x/y symmetry. It is therefore only necessary to calculate RAT at three angles for each wavelength of interest, and to combine them appropriately with the path fractions.¹

In the above example, path fractions are readily calculated by simple geometry [9]. But when the angle of incidence is not normal, or for irregular structures such as random pyramids, it is generally simpler to employ ray tracing to determine the possible paths and their fractions. At the upper extreme, a ray tracing simulation with 100,000 rays impinging on randomly distributed hillocks at $\theta = 20^\circ$ and $\phi = 20^\circ$ finds ~ 350 unique paths; about 165 of these paths account for 99% of rays. The subsequent RAT calculations for all of these paths is necessarily slower than for typical structures, but not debilitating.

In OPAL 1, ray tracing had been performed externally for normally incident light and an ideal ω [1, 2] and the paths were stored in look-up tables. In OPAL 2, the ray tracing is conducted internally. This permits the user to choose any ω , any incident angle, and to include more complicated

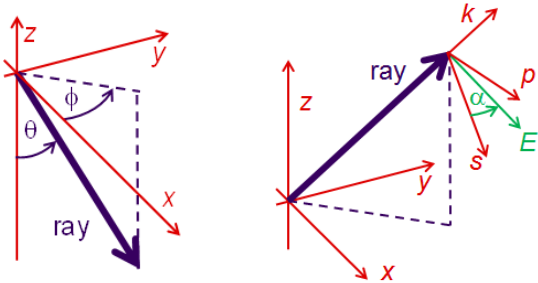


Fig. 1. Coordinate system used in OPAL 2, where θ and ϕ define the incident angle, and α defines the polarization angle.

¹ This approach does not apply to the tracing of transmitted rays within the substrate because refraction depends on wavelength. Also, once transmitted into the substrate, rays can escape from internal boundaries even before passing through the substrate; this possibility is neglected by OPAL 2.

morphologies such as hillocks and planar regions.

The inputs required of the ray tracing component are

- the zenith angle θ to the normal of the plane of the cell, and the azimuth ϕ angle to the [100] crystal axis (Fig. 1);
- the morphology, i.e., the type of texture;
- the characteristic angle ω of the texture, defined in Fig. 2;
- the choice of whether pyramids (or hillocks) are distributed in a random or regular fashion,
- the fraction of the surface that is planar (i.e., untextured).

The planar fraction can either be independent of the texture, as might be the case when representing large regions where texturing failed, or it can be distributed amongst the texture. As illustrated by Fig. 2(d), ‘distributed’ planar regions are defined as surrounding each facet such that rays can bounce from a facet onto a planar region and possibly from there onto a neighboring facet. It is evident that for concave morphologies, such as inverted pyramids or spherical caps, light cannot reflect from a planar region onto a facet (or vice versa) when defined in this way; thus, for these morphologies, distributed and independent planar fractions yield identical results.

With the aforementioned inputs, OPAL 2 employs ray tracing to determine the set of unique paths that the incident light follows. Since RAT is not calculated, since polarization is not monitored, and since the paths are independent of wavelength, the ray tracing is fast. On the current server, 30,000 rays are typically traced in less than 0.3 s.

Fig. 3 presents the results of ray tracing for regular ideal upright pyramids with $\theta = 30^\circ$ and $\phi = 30^\circ$. The figure plots the path fractions, where the symbols are the average of 10 simulations, and the error bars are the 95% confidence interval attained from those 10 simulations. For clarity, only four of the ten unique paths are shown. In this example, we find that after 10,000 rays, the 95% confidence interval is less than $\pm 0.4\%$ (absolute) for every path.

B. Thin-film calculations

Having determined the set of unique paths, the reflection, absorption and transmission (RAT) of each path is calculated. This requires additional inputs:

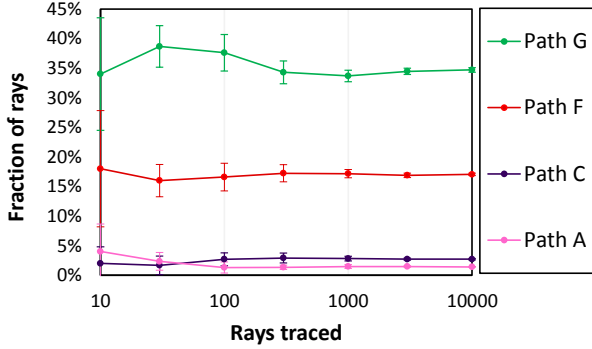


Fig. 3. Fraction of rays vs number of rays traced for 4 of 10 paths for regular upright pyramids with $\theta = 30^\circ$ and $\phi = 30^\circ$. Symbols represent the average of $N = 10$ simulations, error bars are the 95% confidence interval, $2\sigma/\sqrt{N-1}$, where σ is the st. deviation.

- the polarization of the incident light, where one can either select unpolarised light or light polarized at angle α ;
- the number and thickness of any thin-film ARCs, where up to 5 films are permitted;
- the materials of the superstrate, films, and substrate.

As an example, to simulate the optics at the encapsulant–cell interface of a high-efficiency solar cell, one might select EVA as the superstrate, SiN_x as an upper film, SiO_2 as a lower film, and c-Si as the substrate. Or if simulating internal reflection, one might invert the order of the four layers.

OPAL 2 then solves the Fresnel equations to determine RAT at each bounce of each path, and combines them appropriately to determine the total RAT for the incident light. This is performed over a range of wavelengths using $n(\lambda)$ and $k(\lambda)$ stored for each material, or alternatively, customized $n(\lambda)$ and $k(\lambda)$ that have been uploaded. The approach is described in more detail in [2].

In the case of unpolarized light, the program determines RAT at multiple polarization angles α and averages them with equal weighting. We find that for typical conditions of interest to PV cells, unpolarized light is well approximated by the average of 3 uniformly spaced polarization angles (i.e., $\alpha = 0^\circ$, 60° and 120°), but 9 angles gives more accuracy with little cost in processing time (i.e., $\alpha = 0^\circ, 20^\circ, \dots, 140^\circ$, and 160°).

Fig. 4 presents the RAT for the aforementioned example of the high-efficiency solar cell under normally incident light.

C. Current calculations

The purpose of optical simulations is usually to maximize current generation and/or current collection in a solar cell. As well as the RAT determined above, this requires the incident spectrum and a model for the internal optics and/or collection.

In regards to the internal optics employed by OPAL, the user defines an optical width equal to $Z \cdot W$, where Z is the optical pathlength enhancement and W is the width of the substrate. They are then used to determine the generation current J_G ,

$$J_G = q \int I(\lambda) \cdot \cos(\theta) \cdot T(\lambda) \cdot \exp[-\alpha(\lambda) \cdot Z \cdot W] \cdot d\lambda, \quad (1)$$

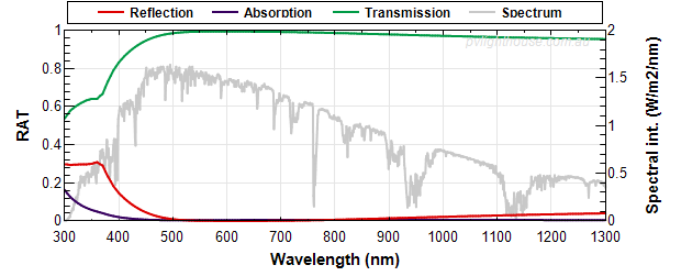


Fig. 4. RAT for the example of the high-efficiency solar cell described in the text. The AM1-5g spectrum is also plotted.

where q is the charge of an electron, $I(\lambda)$ is the photon flux of the incident spectrum under normal incidence, $T(\lambda)$ is the transmission into the substrate, and α is the absorption coefficient of the substrate; the integral is performed over all λ .

OPAL 2 also calculates the equivalent current that is reflected by the cell J_R , and absorbed in the ARC J_A , by replacing $T(\lambda)$ with either $R(\lambda)$ or $A(\lambda)$. In so doing, it calculates the current density that would have been generated in the substrate had it not been reflected or absorbed. This is a more meaningful metric than the commonly used ‘weighted average reflectance’ (WAR), which is the equivalent of arbitrarily defining wavelength limits to the integral and setting the exponential term to unity. (Making the WAR less useful still is that its wavelength limits are not standardized.)

OPAL 2 sums J_R , J_A and J_G to determine the equivalent incident current density J_{inc} . This is the current density that would have been generated in the substrate if there had been no external optical losses at the front surface. Be aware that J_{inc} is dependent on $\alpha(\lambda)$, Z and W .

Thus, one can use OPAL 2 to find an ARC that maximizes J_G for a large variety of morphologies, materials, spectra and incident angles. One can also upload a cell’s $IQE(\lambda)$ to maximize the collection current instead of J_G ; in this case, the $IQE(\lambda)$ should not include the effects of ARC absorption since that is introduced by the OPAL simulations.

Finally, a 1D generation current is determined using models for pyramidal texture [10] and spherical caps [11].

III. HILLOCKS AND SPHERICAL CAPS

Upright pyramids, inverted pyramids and V grooves are well known morphologies that have been assessed in much detail. Two additional morphologies—each with a practical relationship to industrial solar cells—are hillocks and spherical caps. They are illustrated in Figs. 2b and 2c.

A. Hillocks

Hillocks are octagon-based upright pyramids. They have been observed in the IC industry [4, 5] and more recently in the PV industry [3, 12, 13]. They are generally thought to be comprised of eight {567} facets rather than the four {111} facets of the better known square-based upright pyramid. These ‘off-axis’ facets evolve due to the exposure of

‘beveling’ planes at convex corners or the formation of ledges on facets. Their existence has been deduced from angle-dependent reflection measurements [3] and SEM images [4, 5].

As evident in Fig. 2b, a surface cannot be entirely comprised of {567} facets unless the hillocks overlap—as they might in the random texture formed by common alkaline etching. In OPAL 2, however, the space between the {567} facets is assumed planar, and hence the simulation of hillocks has a minimum planar fraction of 8.8%. Alternative approaches to modeling hillocks are intended for future versions.

B. Spherical caps

Spherical caps, depicted in Fig. 2c, are elements of a sphere whose two-dimensional counterpart is a circular segment. In this case, we define ω such that when $\omega = 90^\circ$, the spherical cap is an inverted hemisphere, and when ω approaches 0° , the spherical cap approaches a planar surface.

It has recently been demonstrated that lightly etched isotexture can be well modeled as inverted spherical caps with $\omega \sim 87^\circ$ [7]. It was further found that as the duration of the isotexture increases, the resulting morphology is better modeled as spherical caps with decreasing ω . After extensive etching, ω approaches 0° and the surface is effectively flat.

While determining a set of unique paths is possible for morphologies comprised of discrete facets, such as pyramids, hillocks and V grooves, this is not strictly possible for spherical caps, which have a single and continuous facet. Theoretically, therefore, spherical caps have infinitely many unique paths. OPAL 2 approximates spherical caps by treating them as a user-defined number of concentric sections of a cone.

With the option to simulate spherical caps, OPAL 2 is the first software to permit optical modeling of isotextured solar cells, which comprised >50% of cells manufactured in 2011.

IV. EXAMPLES

A. Variation of the characteristic angle, ω

Optical analyses of pyramidally textured solar cells usually assume that $\omega = \text{atan}(\sqrt{2}) = 54.74^\circ$. This is the angle between the {100} and {111} planes, and can be considered ideal. In practice, however, ω is less than ideal for random pyramids because the ratio of the etch rates for {100} to {111} is never infinite [14]. Experimental ratios between 5 and 200 have been reported [15–17].

OPAL 2 can simulate morphologies over a wide range of ω . It is demonstrated here with four cases: (1) regular upright pyramids, (2) random upright pyramids, (3) random hillocks, and (4) spherical caps. The results are presented in Figs. 5 and 6, which plot the fraction of incident rays that bounce once, twice, thrice, etc., from the front surface as a function of ω .

Figs. 5 and 6 also plot and compare the optical losses as fractions, J_R/J_{inc} and J_A/J_{inc} , where the losses are determined for c-Si cells in air under an unpolarized normally incident AM1-5g spectrum. The cell thickness is $W = 180 \mu\text{m}$ and the

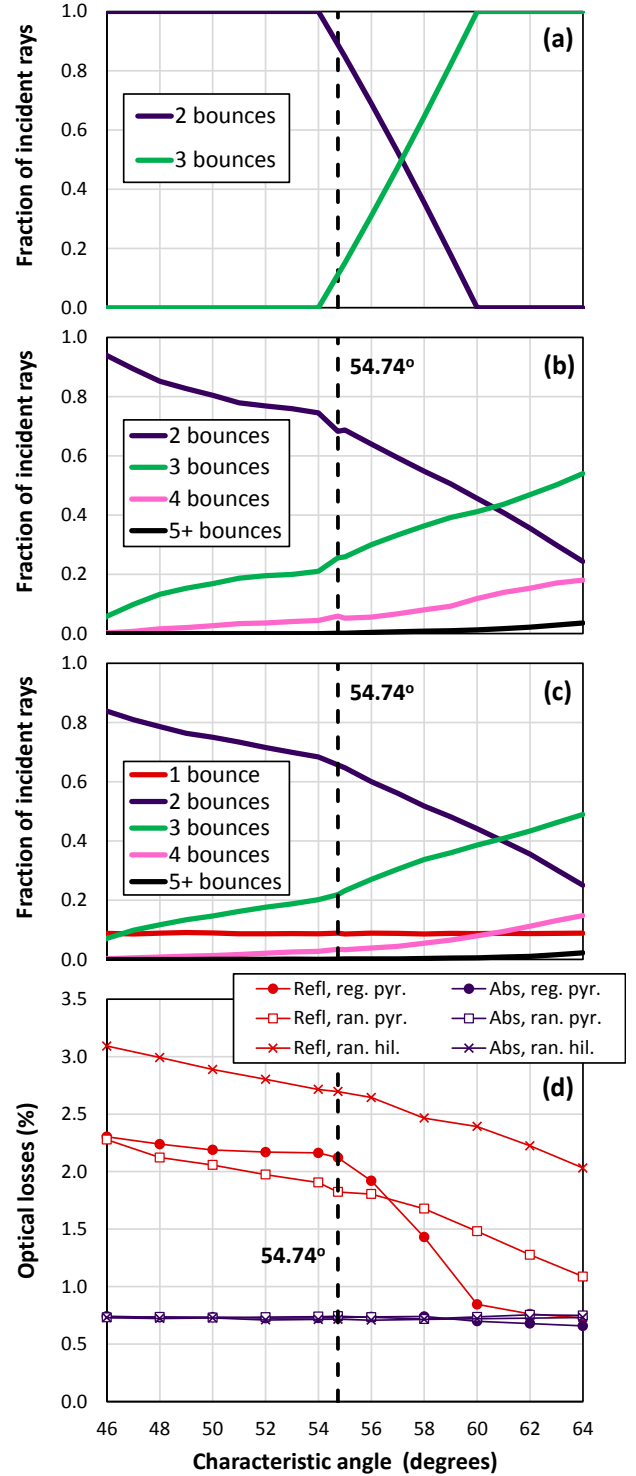


Fig. 5. Fraction of rays that bounce twice, three times, etc., at the front surface of (a) regular upright pyramids, (b) random upright pyramids, and (c) random hillocks as a function of the characteristic angle ω and (d) reflection and absorption vs ω for Cases 1, 2 & 3.

optical enhancement is $Z = 4$ (except for Case 4, when $Z = 2$.) In each simulation, an SiN_x ARC is included; its thickness is set to minimize the optical losses at each ω . The refractive index of SiN_x is taken from [2], which represents a low- n film

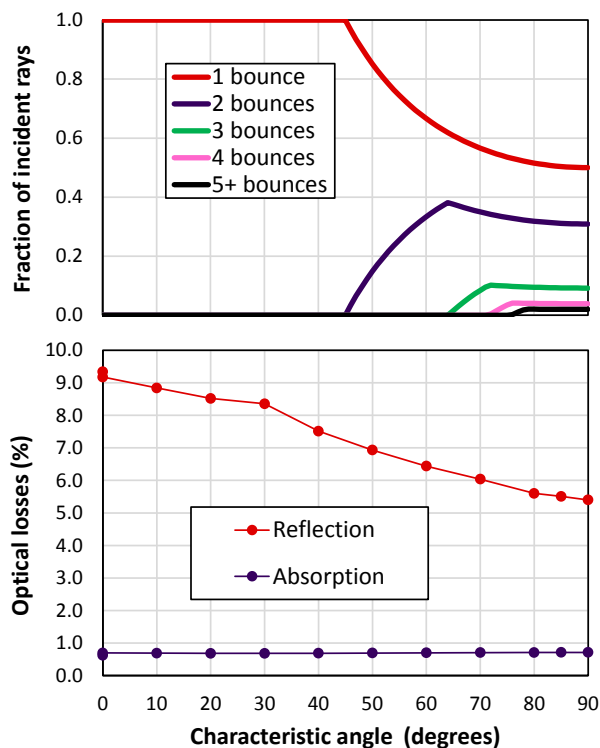


Fig. 6. (a) Fraction of incident rays that bounce once, twice, etc. at the front surface, and (b) reflection and ARC absorption vs ω for spherical caps. Simulation details described in the text.

that provides very good surface passivation [20], and the refractive index of c-Si is taken from [21]. For the random structures, the pyramid/hillock heights differed by at most a factor of 5 and their bases were unaligned [11]. The wavelength was swept in 5 nm intervals from 250 to 1400 nm.

Fig. 5 illustrates that for regular upright pyramids there is only a slight increase in reflection when ω is smaller than the ideal (54.74°). This is because all normally incident rays bounce twice from upright regular pyramids over the range $\omega = 45\text{--}54^\circ$. By contrast, there is a rapid decrease in reflection as ω increases above 54° because an increasing number of rays bounce three times from the pyramid facets [9]. Fig. 6 illustrates that for spherical caps, there is a gradual reduction in reflection as ω increases, as dictated by the gradual increase in the fraction of rays that have multiple bounces (Fig. 6a).

Conclusions regarding the dependence of ray paths on regular structures are not novel and can be deduced with trigonometry; for example the green line in Fig. 5a follows the equation $\cos(5\omega)/\cos(\omega)$ between 54° and 60° [9]. The geometry becomes rather complicated, however, for non-normally incident light and for irregular texture, such as random upright pyramids and hillocks.

Plotting path fractions gives insight into optical losses. The comparison of regular and random pyramids evident in Fig. 5 provides an example. From simple geometry one can deduce that they must be identical at $\omega = 45^\circ$ since all normally incident rays bounce exactly twice from either texture. But as

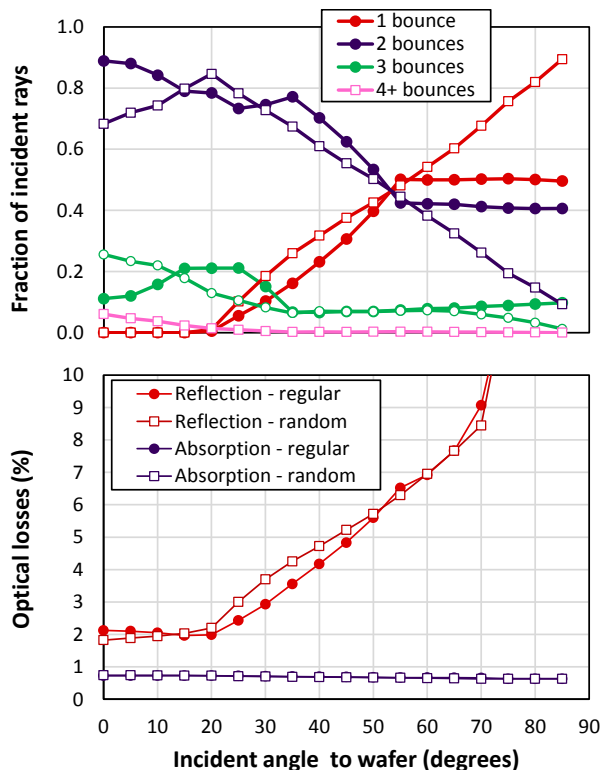


Fig. 7. Optical losses vs θ for $\phi = 0^\circ$ for regular (solid symbols) and random (open symbols) upright pyramids for Case (a) & (b).

ω increases, random texture becomes increasingly superior to regular texture as more and more rays are reflected three times due to glancing bounces from orthogonal pyramids. At approximately the ideal ω of 54.74° , and surreptitiously for industrial c-Si solar cells, random pyramids enjoy their greatest advantage over regular pyramids. (Thus, at this angle, treating random pyramids as regular pyramids incurs the greatest error.) As ω increases further, regular pyramids rapidly become superior as all rays are reflected three times, while random pyramids still allow some rays to reflect twice before ‘escaping’ over smaller pyramids.

It is relevant to note here that within the range of ω observed for experimental alkaline-etched samples ($\omega = 50\text{--}54.74^\circ$ [3]), the reduction in reflection is more severe for random rather than regular pyramids. Many conclusions such as these can be deduced from an optical evaluation of surface morphologies.

B. Angle of incidence

It can also be amusing to assess the losses for non-normal angles of incidence. Fig. 7 plots the losses as a function of θ with $\phi = 0^\circ$ for Cases (a) and (b), which represent regular and random upright pyramids with $\omega = 54.74^\circ$.

Fig. 7 illustrates that the relative advantage or disadvantage of random over regular pyramids varies with θ . The causes of these subtle differences are not expounded here. Of more importance, the figure shows that there is a distinct and rapid increase in optical losses for both morphologies when $\theta > 25^\circ$.

There is a plethora of complicating factors when considering the implications for PV modules: reflection from the glass, absorption in the glass and encapsulant, polarization, azimuth angle, and changes in spectrum and intensity throughout the day and year. Accounting for all of them is a large and tedious undertaking—and one that exceeds the capabilities of OPAL 2. Nevertheless, if one applies Snell's law and assumes planar module surfaces and an encapsulant refractive index of 1.5, then sunlight incident to a module at $< 39.3^\circ$ will be refracted such that its incident angle to the cells is $\theta < 25^\circ$. Thus, for a large fraction of the useful sunlight hours in a day, the relative optical losses of our example remain approximately constant.

C. Independent or distributed planar regions

It is not uncommon for texturing to cover a portion of a wafer and for the remainder to be planar. As described above, OPAL 2 can treat planar regions as being optical independent from the texture, or evenly distributed within the texture. These cases represent the two extremes of how planar regions behave optically on a textured wafer.

When the planar regions are distributed rather than independent, the optical losses are necessarily greater for normally incident light. While each case has the same fraction of rays striking its planar surface, the distributed case reflects some rays from a texture facet onto a planar region and from there into space, negating any possibility of a third bounce. Fig. 8 plots the optical losses for random upright pyramids with Case (b) at $\omega = 54.74^\circ$ under normally incident light.

VI. CONCLUSION

Like Giza, c-Si solar cells are decorated with square-based aligned pyramids of differing heights and elevation but of similar base angles;² and in the case of poor alkaline etching, the pyramids of c-Si solar cells are also surrounded by planar areas. It is of passing interest then that had Cheops and his descendants expanded their necropolis to an effectively infinite extent in the x/y plane, OPAL 2 might now be used by Egyptologists. They would find that it offered a rapid and accurate means to determine the reflection and absorption at Giza under any angle of incidence or polarization, but unlike photovoltaic engineers, they would find no value in its capacity to quantify the optical losses from inverted pyramids, V grooves, hillocks or spherical caps, the last of which simulates the isotexture of mc-Si solar cells.

² The facets of the three main pyramids at Giza are aligned to the cardinal directions; the base angles are 51° , 52° and 53° ; the original heights vary by a factor of 2.2; and there is a spate of small and somewhat ill-formed satellite pyramids similarly aligned. Whether the size and location of the three big pyramids were intended to represent the stars of Orion's belt is a matter of contention, but it *can* be concluded that since they were coated in a radiant white limestone, the Pharaohs did not construct the pyramids to suppress reflection.

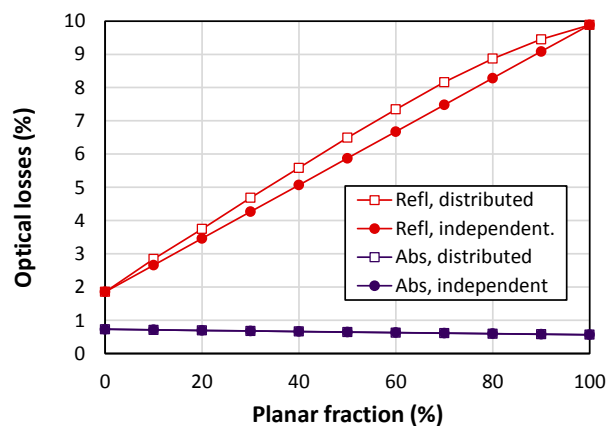


Fig. 8. Optical losses for Case (b) vs the planar fraction for independent and distributed planar regions.

REFERENCES

- [1] S. C. Baker-Finch and K.R. McIntosh, "A freeware optical model for precise optical analysis of the front surface of a solar cell," *35th IEEE Photovoltaic Specialist Conference*, 2010, p. 2184–2187.
- [2] S. C. Baker-Finch and K. R. McIntosh, "Reflection of normally incident light from silicon solar cells with pyramidal texture," *Progress in Photovoltaics*, vol. 19, pp. 406–416, 2011.
- [3] S. C. Baker-Finch and K.R McIntosh, "Reflection distributions of textured monocrystalline silicon: implications for silicon solar cells," *Progress in Photovoltaics: Research and Applications*, Available online, DOI: 10.1002/pip.2186.
- [4] Y. K. Bhatnagar and A. Nathan, "On pyramidal protrusions in anisotropic etching of $<100>$ silicon," *Sensors and Actuators A*, vol. 36, pp. 233–240, 1993.
- [5] S.-S. Tan, M. Reed, H. Han and R. Boudreau, "Morphology of etch hillock defects created during anisotropic etching of silicon," *Journal of Micromechanics and Microengineering*, vol 4, p. 147, 1994.
- [6] Y. Nishimoto, T. Ishihara, and K. Namba, "Investigation of acidic texturization for multicrystalline silicon solar cells," *Journal of the Electrochemical Society*, vol. 146, p. 457–461, 1999.
- [7] S. C. Baker-Finch, K. R. McIntosh and M. L. Terry, "Isotextured silicon solar cell analysis and modeling, 1: Optics," in press, *IEEE Journal of Photovoltaics*, 2012.
- [8] www.pvlighthouse.com.au. Last accessed, 21-May-2012.
- [9] M. A. Green, *Silicon solar cells*, University of New South Wales, 1995, pp. 348–349.
- [10] P. A. Basore, "Numerical modelling of textured silicon solar cells," *IEEE Transactions on Electron Devices*, Vol. 37, pp. 337–343 1990; and P. A. Basore, "Extended spectral analysis of internal quantum efficiency," *23rd IEEE Photovoltaic Specialists Conference*, pp. 147–152, 1993.
- [11] S. C. Baker-Finch, K. R. McIntosh, D. Inns and M. L. Terry, "Modelling isotextured silicon solar cells," this conference, 2012.
- [12] B. Vallejo, M. Gonzalez-Manas, J. Martinez-Lopes and M.A. Caballero, "On the texturization of monocrystalline silicon with sodium carbonate solutions," *Solar Energy*, vol. 81, p. 565, 2007.
- [13] M. Rosa, M. Allegrezza, M. Canino, C. Summonte and A. Desalvo, "TMAH-textured, a-Si/c-Si heterojunction solar cells

- with 10% reflectance,” *Solar Energy Materials and Solar Cells*, vol. 95, pp. 2987–2993, 2011.
- [14] M. A. Green, “Analytical expressions for spectral composition of band photoluminescence from silicon wafers and bricks,” *Applied Physics Letters*, vol. 99, 131112, 2011.
- [15] J. B. Price, “Anisotropic etching of silicon with KOH-H₂O-isopropyl alcohol,” *Semiconductor Silicon*, H. Huff and R. Burgess, eds., pp. 339–353. Electrochemical Society, 1973.
- [16] E. Vazsonyi, K. De Clerq, R. Einhaus, E. Van Kerschaver, K. Said, J. Poortmans, J. Szlufcik and J. Nijs, “Improved anisotropic etching process for industrial texturing of silicon solar cells,” *Solar Energy Materials and Solar Cells*, Vol. 57, pp. 179–188, 1999.
- [17] A. Merlos, M. Acero, M. Bao, J. Bausells and J. Esteve, “TMAH/IPA anisotropic etching characteristics,” *Sensors and Actuators A*, Vol. 37–38, pp. 737–743, 1993.
- [18] M. Sekimua, “Anisotropic etching of surfactant-added TMAH solution,” *IEEE International Conference on Micro Electro Mechanical Systems*, pp. 650–655, 1999.
- [19] R. Wind and M. Hines, “Macroscopic etch anisotropies and microscopic reaction mechanisms: a micromachined structure for the rapid assay of etchant anisotropy,” *Surface Science*, Vol. 460, p. 21, 2000.
- [20] Y. Wan, K. R. McIntosh, A. F. Thomson and A. Cuevas, “Low surface recombination velocity by low-absorption silicon nitride on c-Si,” this conference and invited for submission to *IEEE Journal of Photovoltaics*, 2012.
- [21] M. A. Green, “Self-consistent optical parameters of intrinsic silicon at 300K including temperature coefficients,” *Solar Energy Materials and Solar Cells*, vol. 92, pp. 1305–1310, 2008.